21st Australasian Fluid Mechanics Conference
Adelaide, Australia
10-13 December 2018

Vortex Dynamics on a 2D Curved Surface Using Discrete Exterior Calculus

Pankaj Jagad[1], Mamdouh S. Mohamed[2] and Ravi Samtaney[1]

[1]Mechanical Engineering, Physical Science and Engineering Division
King Abdullah University of Science and Technology, Jeddah, Saudi Arabia

[2]Department of Mechanical Design and Production
Faculty of Engineering, Cairo University, Giza, Egypt

Abstract

We present examples of vortex dynamics on a curved 2D surface using simulations based on the approach of discrete exterior calculus (DEC) developed by Mohamed *et al.* [8]. The DEC method allows a coordinate independent implementation and preserves vector calculus identities discretely. In addition, it has been demonstrated to exhibit good conservation of secondary flow quantities such as kinetic energy (for inviscid flows) and discretely satisfies vorticity conservation both locally and globally. These structure-preserving properties of DEC make it a suitable tool to investigate vortex and vorticity dynamics on 2D curved surfaces. In particular, we focus on the flow past a stationary cylinder (a canonical problem in fluid dynamics) embedded on a sphere (positive Gaussian curvature) or another cylinder (zero Gaussian curvature). We compute quantities of dynamical importance such as the drag coefficient, lift coefficient and Strouhal number. Another example presented is the evolution of initially randomly distributed vortices on a unit sphere in to a quadrupolar vortical structure similar to reported in Dritschel *et al.* [4].

Introduction

Discrete exterior calculus (DEC) is a promising method for investigations of vortex dynamics because of its excellent vorticity preservation property. The latter may be attributed to the fact that DEC discretization preserves discrete analogues of continuous properties of interest [2]. DEC is convenient for solving flows on manifolds / curved surfaces since the discretization is independent of the coordinate system [2]. Scalars, vectors and tensors are the fundamental quantities of interest in interior calculus, whereas differential forms are of interest in exterior calculus. Loosely defined, a form is "something that occurs under an integral sign" [5], e.g., velocity vector integrated over an edge of a triangle represents a 1-form. The discrete counterpart of a continuous manifold is a simplicial complex with a dual mesh associated with it. In two-dimensional case, the primal simplicial complex consists of vertices, edges (the line connecting two vertices), and contiguous triangles (constructed by connecting the edges). The duals associated with them are a polygon (constructed by connecting the circumcenters / barycenters of the triangles associated with the vertex) , dual edges (formed by connecting circumcenters / barycenters straddling the primal edge) and circumcenter/ barycenter of the triangles, respectively. A good literature on the subject can be found in [1, 2, 3, 5, 6, 7, 8, 9, 11]. DEC is capable of well resolving the vortical structures in a flow. The aim of the present study is to demonstrate this ability. We investigate vortex dynamics of a flow past a circular cylinder embedded in a spherical surface as well as in a cylindrical surface using an in-house DEC code [8]. The diameter of the cylinder is assumed to be unity and the radius of both surfaces is 12. Reynolds numbers of 40 and 100 are employed. A second example presented is the long time evolution of initially randomly distributed vortical structures on a unit sphere.

Governing Equations

The governing equations for fluid motion are surface Navier-Stokes equations, expressed as (for an incompressible flow and constant viscosity) [10]

$$\frac{\partial \mathbf{v}}{\partial t} - \mu \left[-\Delta^{dR}\mathbf{v} + 2\kappa\mathbf{v} \right] + \nabla_{\mathbf{v}}\mathbf{v} + grad_S p = 0, \tag{1}$$

$$div_S \mathbf{v} = 0, \tag{2}$$

where $\mathbf{v}$ is the tangential surface velocity, μ is the dynamic viscosity, p is the surface pressure, $\nabla_{\mathbf{v}}$ is the covariant directional derivative, $grad_S$ is the surface gradient, div_S is the surface divergence, Δ^{dR} is the surface Laplace-DeRham operator, and κ is the Gaussian curvature. The Gaussian curvature term and the Laplace-DeRham operator result from the divergence of the deformation tensor and the non-commutativity of the second covariant derivative in curved spaces [10]. The covariant formulation of equations (1) and (2) reads [10]

$$\frac{\partial \mathbf{u}}{\partial t} - \mu[*d*d\mathbf{u} + 2\kappa\mathbf{u}] + \nabla_{\mathbf{v}}\mathbf{u} + dp = 0, \tag{3}$$

$$*d*\mathbf{u} = 0, \tag{4}$$

where $\mathbf{u}$ is the 1-form velocity, $*$ is the Hodge star, and d is the exterior derivative. The covariant derivative can be expressed as [8]

$$\nabla_{\mathbf{v}}\mathbf{u} = \mathcal{L}_{\mathbf{v}}\mathbf{u} - \frac{1}{2}d\left(\mathbf{u}\left(\mathbf{v}\right)\right). \tag{5}$$

The Lie derivative term is expressed as [8]

$$\mathcal{L}_{\mathbf{v}}\mathbf{u} = d\left(\mathbf{u}\left(\mathbf{v}\right)\right) + i_{\mathbf{v}}d\mathbf{u}, \tag{6}$$

where $i_X\alpha$ is the interior product of a k-form α with a vector field $\mathbf{x}$, which can be expressed as [8]

$$i_{\mathbf{x}}\alpha = (-1)^{k(N-k)} * \left(*\alpha \wedge \mathbf{x}^{\flat} \right), \tag{7}$$

where $\wedge$ stands for the wedge product, N stands for the space dimension, and $\mathbf{x}^{\flat}$ is a form which corresponds to the vector field $\mathbf{x}$. Substituting equations (5) - (7), and defining dynamic pressure 0-form as $p^d = p + \frac{1}{2}\left(\mathbf{u}\left(\mathbf{v}\right)\right)$, equation (3) (in two-dimensions) reads

$$\frac{\partial \mathbf{u}}{\partial t} - \mu * d * d\mathbf{u} - 2\mu\kappa\mathbf{u} + *\left(\mathbf{u} \wedge *d\mathbf{u}\right) + dp^d = 0. \tag{8}$$

Considering the primal mesh for the domain discretization and the corresponding dual mesh, and with a choice of the velocity 1-form $\mathbf{u}$ on the dual edges, except at the first position in the wedge product where the choice has to be on the primal edge (this choice represents tangential velocity 1-form) for consistency [8], the discrete governing linear momentum and continuity equations in DEC notation read

$$-\frac{(U^*)^{n+1}-(U^*)^n}{\triangle t}+\mu d_0 *_0^{-1}\left[\left[-d_0^T\right]*_1 (U^*)^{n+1}+d_b\,(V)^n\right]$$

$$+2\mu\kappa(U^*)^{n+1}-(W_V)^n *_0^{-1}\left[\left[-d_0^T\right]*_1 (U^*)^n+d_b\,(V)^n\right]$$

$$+*_1^{-1} d_1^T\left(P^d\right)^{n+1}=0, \tag{9}$$

$$d_1\,(U^*)^{n+1}=0. \tag{10}$$

Here, U^* represent the vector containing mass flux $u^*=*_1^{-1}\mathbf{u}$ through the primal edges, the superscript $n+1$ stands for the current time step, and n stand for the previous time step (the viscous and curvature terms are implicit, whereas the convection term is explicit). The W_V matrix represents the discrete wedge product of the tangential velocity 1-form with the 0-form $*$du (as in equation (8)) and contains the values of the tangential velocity 1-form. The details of the discrete operators used in these equations can be found in [8]. Equations (9) and (10) are solved simultaneously for U^* and p^d.

Flow Past a Cylinder Embedded on Spherical and Cylindrical Surfaces

Computational Domain

The computational domain consists of a circular contour, representing a circular cylinder, embedded on a spherical surface, as shown in figure 1. The diameter (D) of the cylinder is unity and radius of the spherical surface is 12. The domain length upstream and downstream of the cylinder are 10 and 60 respectively. The domain width on either side of the cylinder is 10. Similar domain dimensions are used for the case of flow past a cylinder embedded in a cylindrical surface.

The boundary conditions are shown in figure 1. At inlet, uniform normal velocity $u=1$, and tangential velocity $v=0$ are assumed. The normal gradients $\partial u/\partial n=0$ and $\partial v/\partial n=0$ are assumed at the outlet. No slip condition, i.e., $u=0$ and $v=0$ is assumed on the cylinder wall. The free-slip condition, i.e., $u=0$ and $\partial v/\partial n=0$, is assumed at the lateral boundaries. The notion of a "far field" outflow boundary condition is somewhat complicated on a curved manifold especially for a spherical or cylindrical surface where extending the outflow boundary to larger distances implies that it eventually runs into the issue that the domain closes in upon itself. This issue may be avoidable by assuming a "branch-cut" of some sorts. Here we simply note that an extensive discussion of these issues is beyond the scope of the present paper.

A sample mesh consisting of 79920 nodes and 159104 triangular elements is shown in figure 2 with clustering of mesh to have the highest resolution (smallest elements) on the cylinder and in the wake. The mesh size adopted for the simulations discussed presently results in a well-resolved mesh independent solution insofar as the quantities of interest (lift, drag etc.) are concerned.

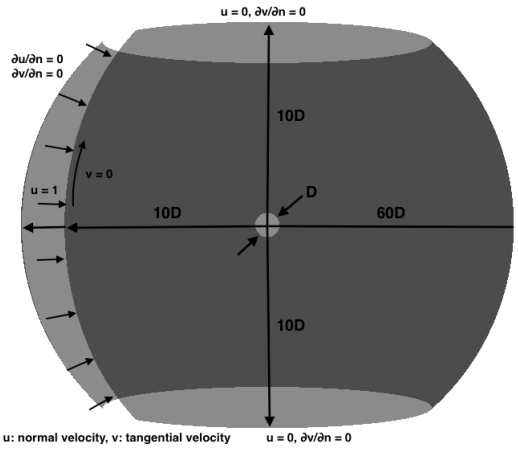

Figure 1: The computational domain

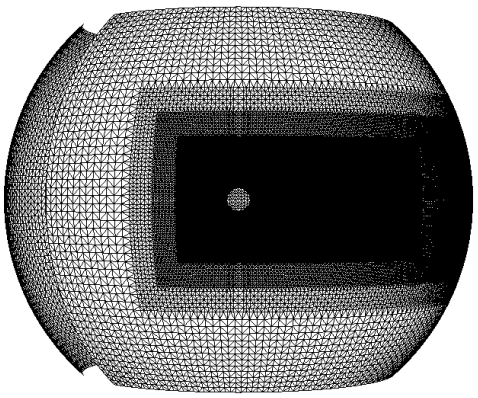

Figure 2: A sample mesh

Vorticity in the Wake

We examine flow past the cylinder at two (relatively low) Reynolds numbers (defining $Re=\rho V_{in}D/\mu$, where ρ, V_{in}, D, and μ stand for the fluid density, the domain inlet velocity, the cylinder diameter, and the fluid dynamic viscosity): $Re=40$ and $Re=100$. In the former case, the Reynolds number is below the critical value for a planar flow and one expects a steady solution with attached vortices on the cylinder. In the latter case, we expect to see periodic vortex shedding and formation of a Karman vortex street. For the $Re=40$ case the vorticity contours are shown in figures 3a and 3b for both the spherical and cylindrical surfaces, respectively. The figure shows the two time instances after the steady state is reached and no variation in time in the solution is noted. The steady state solution comprises of a pair of attached vortices of opposite signs behind the cylinder similar to that for flow past a cylinder in flat planar 2D geometry.

For the higher $Re=100$ cases, snapshots in time of the vorticity contours for both spherical and cylindrical surfaces are shown Figures 4a and 4b, respectively. As can be noticed for both cases, the flow exhibits a vortex shedding in the wake behind the cylinder. These observations regarding the vortical structures are similar to that for the flow past a cylinder embedded on a flat surface.

Computation of the Force on the Cylinder

The net force on the cylinder is expressed as $\vec{F}=\int_S -p\vec{n}dA+$

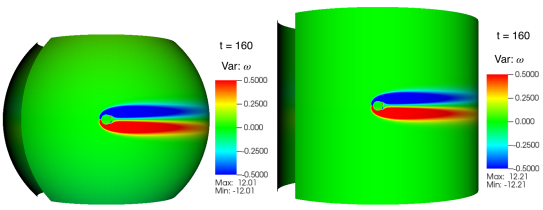

(a) Spherical surface (b) Cylindrical surface

Figure 3: Contour plots of vorticity at Re = 40.

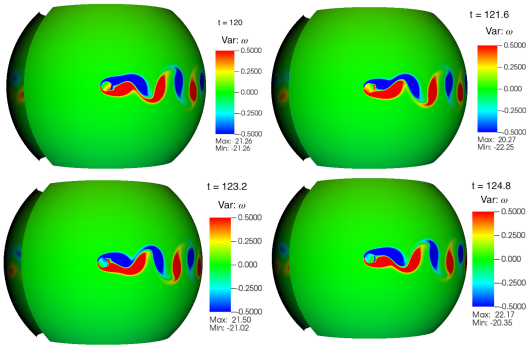

(a) Spherical surface

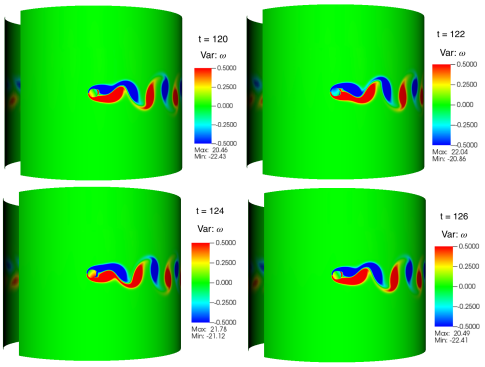

(b) Cylindrical surface

Figure 4: Contour plots of vorticity at Re = 100.

$\mu \int_S \vec{\omega} \times \vec{n} dA$ [12], where p, $\vec{n}$, $\vec{\omega}$, dA, and S stand for the pressure, the unit outward facing normal to the cylinder, the vorticity vector, an infinitesimally small area on the cylinder surface and the total surface area of the cylinder (the circumference of the circle / contour which corresponds to the cylinder). Since the cylinder is discretized into N edges, the discrete expression of the force vector is $\vec{F} = \sum_{k=1}^{N} (-p\vec{n}dA)_k + \mu \sum_{k=1}^{N} (\vec{\omega} \times \vec{n} dA)_k$, where the subscript k stands for the k-th edge. The drag force F_d and the lift force F_l are respectively the x and y components of the force vector.

Drag Coefficient (C_d), Lift Coefficient (C_l), and Strouhal Number (St)

The definitions of these parameters are: the drag coefficient $C_d = F_d / \left(\frac{1}{2}\rho V_{in}^2 D\right)$, the lift coefficient $C_l = F_l / \left(\frac{1}{2}\rho V_{in}^2 D\right)$, and the Strouhal number $St = fD/V_{in}$, where f denotes the vortex shedding frequency. The plots of drag and lift coefficients (at $Re = 100$) as a function of time are shown in figure 5a for the spherical surface and in figure 5b for the cylindrical surface. The corresponding values are reported in table 1. The mean values of the drag coefficient for the flow over spherical surface are found to be 1.571 and 1.37 at Reynolds number of 40 and

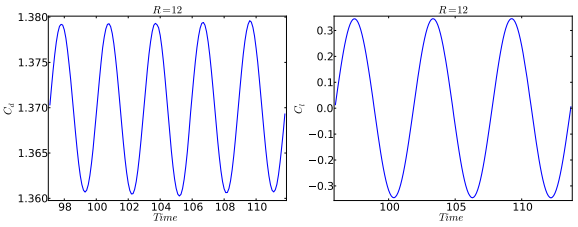

(a) Spherical surface

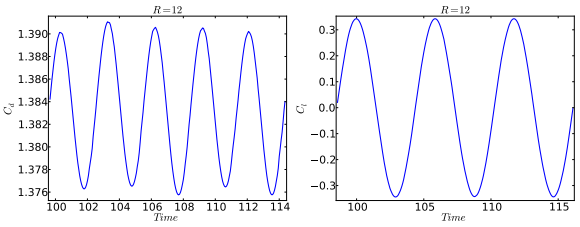

(b) Cylindrical surface

Figure 5: Drag and lift coefficients as a function of time, Re = 100

Surface type	Reynolds number	C_d (mean)	C_l (rms)	St
Spherical ($R = 12$)	40	1.571	-	-
	100	1.370	0.244	0.169
Cylindrical ($R = 12$)	40	1.605	-	-
	100	1.384	0.243	0.171

Table 1: Values of the drag coefficient, lift coefficient, and Strouhal number

100 respectively. For the flow over cylindrical surface, they are found to be 1.605 and 1.384 respectively at Reynolds number of 40 and 100. At Reynolds number of 100, the root mean square (rms) value of the lift coefficient and the Strouhal number are computed to be 0.244 and 0.169, respectively, for the spherical surface and they are computed to be 0.243 and 0.171, respectively, for the cylindrical surface.

Evolution of Vortical Structures on a Sphere from a Random Initial Condition

We consider two cases here: (i) random initial location of the vortices each of constant strength, and (ii) random initial location of the vortices with random strength. In each case, 200 initial vortices are considered on a unit sphere. The initial vorticity distribution is expressed as $\omega = \Gamma / \cosh^2(3r/a)$, where Γ, a, and r stand for the vortex strength, the vortex radius and the distance between any field point and the vortex center. For the former case, a constant strength $\Gamma = \pm 3$ is chosen for all vor-

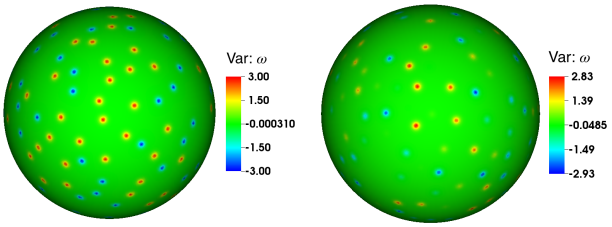

(a) Constant strength (b) Random strength

Figure 6: Initial vortices on the unit sphere

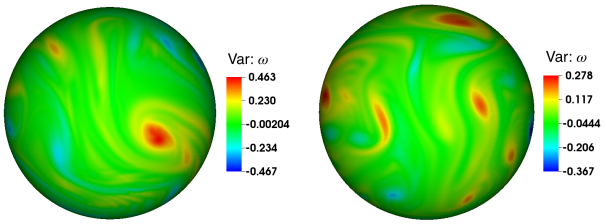

(a) Constant initial strength (b) Random initial strength

Figure 7: Vortical structures at time t = 200

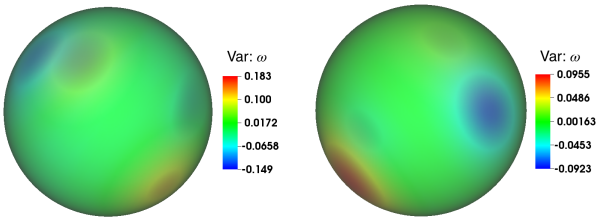

(a) Constant initial strength (b) Random initial strength

Figure 8: Quadrupolar vortical structure at time t = 2000

tices. For the later case, a random strength between -3 and 3 is considered. The vortex radius $a = 0.075$ is chosen for both the cases. The aforementioned governing equations are solved assuming the viscosity $\mu = 10^{-5}$. The initial vortices are shown in figure 6. As the solution evolves, the like-signed vortices merge together to form large scale structures (see figure 7). At late times, a quadrupolar vortical structure is formed as shown in figure 8 . This quadrupolar structure is similar to that reported in Dritschel et al. [4] obtained using geodesic grid method (GGM) and combined Lagrangian advection method (CLAM). The evolution of the solution into quadrupolar vortical structure at late times demonstrates the ability of the DEC method.

Conclusions

The potential of DEC for studying vortex dynamics on curved surfaces is demonstrated by solving (i) two-dimensional flows past a cylinder embedded in spherical and cylindrical surfaces, and (ii) vortical structures on a unit sphere. For the former problem, for Reynolds number of 40, there is a pair of attached vortices of opposite sign found behind the cylinder, which is akin to the case of flow past a cylinder embedded on a flat surface. A vortex street is present in the wake behind the cylinder at Reynolds number of 100 similar to the case of flat surface flow past a cylinder. The values of drag coefficient, lift coefficient and Strouhal number are determined for the cases presented. For the latter problem, a quadrupolar vortical structure is formed at late times, which is similar to that reported in the literature.

References

[1] Desbrun, M., Hirani, A. and Marsden, J., Discrete exterior calculus for variational problems in computer vision and graphics, in *Decision and Control, 2003. Proceedings. 42nd IEEE Conference on*, IEEE, 2003, volume 5, 4902–4907, 4902–4907.

[2] Desbrun, M., Hirani, A. N., Leok, M. and Marsden, J. E., Discrete exterior calculus, *arXiv preprint math/0508341*.

[3] Desbrun, M., Kanso, E. and Tong, Y., Discrete differential forms for computational modeling, in *Discrete differential geometry*, Springer, 2008, 287–324.

[4] Dritschel, D. G., Qi, W. and Marston, J., On the late-time behaviour of a bounded, inviscid two-dimensional flow, *Journal of Fluid Mechanics*, **783**, 2015, 1–22.

[5] Flanders, H., *Differential Forms with Applications to the Physical Sciences by Harley Flanders*, volume 11, Elsevier, 1963.

[6] Hirani, A. N., *Discrete exterior calculus*, Ph.D. thesis, California Institute of Technology, 2003.

[7] Hirani, A. N., Nakshatrala, K. B. and Chaudhry, J. H., Numerical method for darcy flow derived using discrete exterior calculus, *arXiv preprint arXiv:0810.3434*.

[8] Mohamed, M. S., Hirani, A. N. and Samtaney, R., Discrete exterior calculus discretization of incompressible Navier-Stokes equations over surface simplicial meshes, *Journal of Computational Physics*, **312**, 2016, 175–191.

[9] Mohamed, M. S., Hirani, A. N. and Samtaney, R., Numerical convergence of discrete exterior calculus on arbitrary surface meshes, *International Journal for Computational Methods in Engineering Science and Mechanics*, 1–13.

[10] Nitschke, I., Reuther, S. and Voigt, A., Discrete exterior calculus (dec) for the surface navier-stokes equation, in *Transport Processes at Fluidic Interfaces*, Springer, 2017, 177–197.

[11] Perot, J. B. and Zusi, C. J., Differential forms for scientists and engineers, *Journal of Computational Physics*, **257**, 2014, 1373–1393.

[12] Shi, J. M., Gerlach, D., Breuer, M., Biswas, G. and Durst, F., Heating effect on steady and unsteady horizontal laminar flow of air past a circular cylinder, *Physics of Fluids*, **16**, 2004, 4331–4345.